Available online at www.sciencedirect.com
ScienceDirect
International Journal of Heat and Mass Transfer 50 (2007) 4265–4274
International Journal of HEAT and MASS TRANSFER
www.elsevier.com/locate/ijhmt

Jet impingement interaction with cross flow in horizontal porous layer under thermal non-equilibrium conditions

Nawaf H. Saeid *

School of Mechanical Engineering, The University of Nottingham Malaysia Campus, 43500 Semenyih, Selangor, Malaysia

Received 22 August 2006; received in revised form 25 January 2007
Available online 30 April 2007

Abstract

In the present article the jet impingement cooling of heated portion of a horizontal surface immersed in a thermally non-equilibrium porous layer is considered for investigation numerically with the presence of a cross flow. The mathematical model is derived for steady, two-dimensional laminar flow based on Darcy model and two-energy equation for fluid and solid phases. A parametric study is carried out by varying the following parameters: cross flow to jet flow velocity ratio parameter ($0 \leqslant M \leqslant 1$); porosity scaled thermal conductivity ratio parameter ($0.1 \leqslant K_r \leqslant 1000$); heat transfer coefficient parameter ($0.1 \leqslant H \leqslant 1000$); Péclet number ($1 \leqslant Pe \leqslant 1000$) and Rayleigh number ($10 \leqslant Ra \leqslant 100$). The total average Nusselt number is defined based on the overall thermal conductivity, which is assumed to be the arithmetic mean of the porosity scaled thermal conductivity of the fluid and solid phases. The total average Nusselt number as well as the average Nusselt number for both fluid and solid phases is presented for different governing parameters. It is found that the presence of a weak cross flow in a jet impinging jet may degrade the heat transfer. The results show that the average Nusselt number calculated from the thermal equilibrium model are the maximum possible values and these values can be reproduced by large values of $H \times K_r$.

1. Introduction

It is well known that cooling a heated surface using jet impingement is more effective than the parallel flow and is usually used in many industrial applications. The characteristics of the jet impingement cooling through horizontal porous layer are important from theoretical as well as application points of view. In general, convection in porous media has received considerable attention from many researchers due to its wide engineering applications. Representative studies participating to convection in porous media in general can be found in the recent books [1–4].

Although the literature shows that the jet impingement through pure (non-porous) fluid has been studies extensively (see, for example, [5–10]) with the presence of cross flow and without it, but it is noticeable that the jet impingement cooling through porous medium has received relatively less attention.

Fu and Huang [11] investigated numerically the effects of a laminar jet on the heat transfer performance of three different shape (rectangle, convex and concave) porous blocks mounted on a heated plate. Their results for forced convection mode show that the heat transfer is mainly affected by a fluid flowing near the heated region. For a lower porous block, the three types of porous block enhance the heat transfer. However, for a higher porous block, the concave porous block only enhances heat transfer. Prakash et al. [12] carried out a detailed flow visualization experiment to investigate the effect of a porous layer on flow patterns without heat transfer. In this study [12] the effect the jet Reynolds number, the permeability of the porous foam, the thickness of the porous foam and the height of the overlying fluid layer are examined. Jeng and Tzeng [13] studied numerically the air jet impingement

* Tel.: +60 3 89248184; fax: +60 3 89248017.
E-mail address: n_h_saeid@yahoo.com

0017-9310/$ - see front matter © 2007 Elsevier Ltd. All rights reserved.
doi:10.1016/j.ijheatmasstransfer.2007.02.025

Nomenclature

c_p	specific heat, J kg^{-1} K^{-1}
d	half of the width of the jet, Fig. 1, m
g	gravitational acceleration, m s^{-2}
h	volumetric heat transfer coefficient between the solid and fluid in the porous media, W m^{-3} K^{-1}
H	heat transfer coefficient parameter, defined in Eq. (10)
k	thermal conductivity, W m^{-1} K^{-1}
K	permeability of the porous medium, m^2
K_r	thermal conductivity ratio parameter, defined in Eq. (10)
L	half of the heat source length, Fig. 1
M	cross flow to jet flow velocity ratio, $M = U_\infty/V_0$
Nu	local Nusselt number along the heat source, Eq. (11)
$\overline{Nu}$	average Nusselt number along the heat source, Eq. (12)
Pe	Péclet number, $Pe = V_0 L/\alpha$
q''	heat flux, W m^{-2}
Ra	Rayleigh number for porous medium, $Ra = g\beta K(T_h - T_c)L/\upsilon\alpha$
s	distance from the heated portion to the end of the solution domain, Fig. 1, m
S	non-dimensional distance (s/L)
T	temperature, K
u, v	velocity components along x- and y-axes, respectively, m s^{-1}
V_0	jet velocity, m s^{-1}
U_∞	inlet cross flow velocity, m s^{-1}
U, V	non-dimensional velocity components along X- and Y-axes, respectively
x, y	Cartesian coordinates, m
X, Y	non-dimensional Cartesian coordinates (x/L, y/L)

Greek symbols

α	thermal diffusivity, $\alpha = (\rho c_p/k)$, m^2 s^{-1}
β	coefficient of thermal expansion, K^{-1}
θ	non-dimensional temperature
υ	kinematic viscosity, m^2 s^{-1}
ρ	density, kg m^{-3}
ϕ	general dependent variable which can stands for θ_f, θ_s or Ψ
φ	porosity, (void volume/total volume of the porous medium)
Ψ	non-dimensional stream function

Subscripts

c	cold wall
h	hot wall
f	fluid
s	solid
t	total (fluid + solid)

cooling of a porous metallic foam heat sink in the forced convection mode. They found the porous Aluminum foam heat sink could enhance the heat transfer from the heated horizontal source by impinging cooling. Their results show that the heat transfer performance of the Aluminum foam heat sink is 2–3 times larger than that without it. Recently Saeid and Mohamad [14,15] presented the thermal performance of the jet impingement cooling in porous media in the mixed convection regime without the presence of the cross flow. Their results show that increasing either the Rayleigh number or jet width lead to increase the average Nusselt number for high values of Péclet number. Narrowing the distance between the jet and the heated portion could increase the average Nusselt number as well. Saeid and Mohamad [14] indicated that no steady-state solution could be found in some cases; when the external jet flow and the flow due to buoyancy are in conflict for domination. The present investigation is an extension of [14,15] with the presence of the cross flow and for local thermally non-equilibrium porous layer.

It should be noted here that the local thermal equilibrium in convection in porous media is not valid for many cases as reported by various authors for different applications [3,16,17]. Schumann [18] suggested a simple two-equation model to account for non-equilibrium condition for incompressible forced flow in a porous medium. Vafai and Sozen [17], extended the Schumann model to account for compressible flow taking into account of Forchheimer term and conduction effects in the gas and solid phases. Recently the non-equilibrium model has been used in the analysis of different convection heat transfer problems in porous media by various authors [19–28]. In the non-equilibrium modeling, it is required to know the volumetric heat transfer coefficient between solid and fluid phases. In fact, the volumetric heat transfer coefficient values depend on the accuracy of the model assumptions and accuracy of the input parameters, such as thermo-physical properties of the solid matrix, effective thermal conductivity, boundary conditions and effect of radiation, etc.

In the present study, the effect of the cross flow on the jet impingement cooling of heated horizontal surface immersed in a fluid saturated porous media is considered as shown in Fig. 1. The fluid saturated the porous media moving at a certain velocity, which can be lower or higher than the velocity of the injected jet. Such flows are of interest to engineers, for instance in cooling of electronic components, paper drying, food industry and agricultural products. The heated segment is assumed to be two times the porous layer thickness, while the jet width is typically small comparing with the porous layer thickness, it is

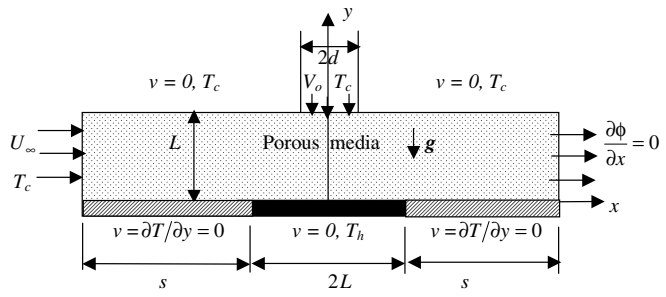

Fig. 1. Schematic diagram of the physical model and coordinate system.

assumed to be ($d/L = 0.1$). The objective of the present study is to characterize the thermal performance of the jet impingement cooling in thermally non-equilibrium porous layer in the mixed convection regime with the limitation of the Darcy model.

2. Governing equations

Fig. 1 illustrates the physical configuration of the present study. The flow velocity in the porous layer is assumed to be very low, therefore, the Darcy's law is assumed to hold and the thermal dispersion can be ignored. The Oberbeck–Boussinesq approximation is used for the fluid density–temperature relationship. With these assumptions, the continuity, Darcy and energy equation for steady, two-dimensional laminar flow in an isotropic and homogeneous porous medium, using the thermally non-equilibrium model are:

$$\frac{\partial u}{\partial x}+\frac{\partial v}{\partial y}=0 \tag{1}$$

$$\frac{\partial u}{\partial y}-\frac{\partial v}{\partial x}=\frac{-g\beta K}{\upsilon}\frac{\partial T_{\mathrm{f}}}{\partial y} \tag{2}$$

$$(\rho c_p)_{\mathrm{f}}\left(u\frac{\partial T_{\mathrm{f}}}{\partial x}+v\frac{\partial T_{\mathrm{f}}}{\partial y}\right)=\varphi k_{\mathrm{f}}\left(\frac{\partial^2 T_{\mathrm{f}}}{\partial x^2}+\frac{\partial^2 T_{\mathrm{f}}}{\partial y^2}\right)+h(T_{\mathrm{s}}-T_{\mathrm{f}}) \tag{3}$$

$$(1-\varphi)k_{\mathrm{s}}\left(\frac{\partial^2 T_{\mathrm{s}}}{\partial x^2}+\frac{\partial^2 T_{\mathrm{s}}}{\partial y^2}\right)+h(T_{\mathrm{f}}-T_{\mathrm{s}})=0 \tag{4}$$

where u, v are the Darcy's velocity components along x- and y-axes, T_{f} is the fluid phase temperature, T_{s} is the solid phase temperature and the other symbols are defined in the nomenclature. Eqs. (1)–(4) and the boundary conditions may be written in dimensionless forms using the following non-dimensional variables:

$$U=\frac{u}{V_0}=\frac{\partial \Psi}{\partial Y};\quad V=\frac{v}{V_0}=\frac{-\partial \Psi}{\partial X};\quad \theta_{\mathrm{f}}=\frac{T_{\mathrm{f}}-T_{\mathrm{c}}}{\Delta T};$$
$$\theta_{\mathrm{s}}=\frac{T_{\mathrm{s}}-T_{\mathrm{c}}}{\Delta T};\quad M=\frac{U_\infty}{V_0} \tag{5}$$

where $\Delta T=(T_{\mathrm{h}}-T_{\mathrm{c}})$ together with non-dimensionalization of all the lengths based on the porous layer thickness (L) and denoting them by respective capital letters leads to the following dimensionless forms of the governing equations:

$$\frac{\partial^2 \Psi}{\partial Y^2}+\frac{\partial^2 \Psi}{\partial X^2}=\frac{-Ra}{Pe}\frac{\partial \theta_{\mathrm{f}}}{\partial X} \tag{6}$$

$$Pe\left(\frac{\partial \Psi}{\partial Y}\frac{\partial \theta_{\mathrm{f}}}{\partial X}-\frac{\partial \Psi}{\partial X}\frac{\partial \theta_{\mathrm{f}}}{\partial Y}\right)=\left(\frac{\partial^2 \theta_{\mathrm{f}}}{\partial X^2}+\frac{\partial^2 \theta_{\mathrm{f}}}{\partial Y^2}\right)+H(\theta_{\mathrm{s}}-\theta_{\mathrm{f}}) \tag{7}$$

$$\frac{\partial^2 \theta_{\mathrm{s}}}{\partial X^2}+\frac{\partial^2 \theta_{\mathrm{s}}}{\partial Y^2}+HK_{\mathrm{r}}(\theta_{\mathrm{f}}-\theta_{\mathrm{s}})=0 \tag{8}$$

The boundary conditions for $M=0$ are defined in Ref. [14]. In the present study the local thermal equilibrium approximation is used in the boundary conditions. For $M>0$, the boundary conditions are:

$$\text{at } X=-(1+S):\ \Psi=MY,\quad \theta_{\mathrm{f}}=\theta_{\mathrm{s}}=0 \tag{9a}$$

$$\text{at } X=(1+S):\ \frac{\partial \phi}{\partial X}=0 \tag{9b}$$

$$\text{at } Y=0:\ \Psi=0,\ \theta_{\mathrm{f}}=\theta_{\mathrm{s}}=1\quad \text{for } -1\leqslant X\leqslant 1$$
$$\text{and otherwise } \frac{\partial \theta_{\mathrm{f}}}{\partial Y}=\frac{\partial \theta_{\mathrm{s}}}{\partial Y}=0 \tag{9c}$$

$$\text{at } Y=1:\ \theta_{\mathrm{f}}=\theta_{\mathrm{s}}=0,\ \Psi=M\quad \text{for } -(1+S)\leqslant X<-D,$$
$$\Psi=X\quad \text{for } -D\leqslant X\leqslant D \text{ and}$$
$$\Psi=M+2D\quad \text{for } D<X\leqslant(1+S) \tag{9d}$$

where, the parameters arise in the non-dimensionlization are defined as:

$$Ra=\frac{g\beta K\Delta TL}{\varphi\upsilon\alpha_{\mathrm{f}}};\quad Pe=\frac{V_0 L}{\varphi\alpha_{\mathrm{f}}};\quad K_{\mathrm{r}}=\frac{\varphi k_{\mathrm{f}}}{(1-\varphi)k_{\mathrm{s}}};\quad H=\frac{hL^2}{\varphi k_{\mathrm{f}}} \tag{10}$$

It is assumed that the fluid and solid phases have the same temperature at the boundaries, i.e., equilibrium conditions. The physical quantities of interest are the local and average Nusselt number for the fluid and solid phases at the heated wall segment, defined by:

$$Nu_{\mathrm{f}}=\frac{q''_{\mathrm{f}}L}{k_{\mathrm{f}}\Delta T}=-\left(\frac{\partial \theta_{\mathrm{f}}}{\partial Y}\right)_{Y=0};\quad Nu_{\mathrm{f}}=\frac{q''_{\mathrm{s}}L}{k_{\mathrm{s}}\Delta T}=-\left(\frac{\partial \theta_{\mathrm{s}}}{\partial Y}\right)_{Y=0} \tag{11}$$

$$\overline{Nu}_{\mathrm{f}}=\frac{1}{2}\int_{-1}^{1}-\left(\frac{\partial \theta_{\mathrm{f}}}{\partial Y}\right)_{Y=0}\mathrm{d}X;\quad \overline{Nu}_{\mathrm{s}}=\frac{1}{2}\int_{-1}^{1}-\left(\frac{\partial \theta_{\mathrm{s}}}{\partial Y}\right)_{Y=0}\mathrm{d}X \tag{12}$$

3. Numerical scheme

Eqs. (6)–(8) subjected to the boundary conditions (9) are integrated numerically using the finite volume method [29,30]. The solution domain, therefore, consists of grid points at which the discretization equations are applied. The upper boundary has the jet inlet and the heat source is located on the lower boundary as shown in Fig. 1. Therefore, the regions near both the upper and lower boundaries are important regions and, therefore, a uniform grid has been selected in Y direction. Non-uniform grid has been

selected in X direction such that the grid points clustered near the center of the jet (Y-axis) where steep variations of the dependent variables are expected. The locations of the faces of the control volumes starting from the inlet of the cross flow $X = -(1+S)$ to the Y-axis are defined as:

$$X(i) = -(1+S) + (1+S)\sqrt{\frac{i-1}{N-1}} \quad i = 1, 2, \ldots, N \tag{13}$$

where N is the half of the total number of the grid points in the horizontal direction. The locations of the grid points are then calculated to be in the center of the control volumes. In the positive X direction the same mesh is reflected as if there is a mirror in the y-axis. The resulting algebraic equations were solved by line-by-line using the Tri-Diagonal Matrix Algorithm iteration. The iteration process is terminated under the following condition:

$$\sum_{i,j} \left| \phi^{n}_{i,j} - \phi^{n-1}_{i,j} \right| \Big/ \sum_{i,j} \left| \phi^{n}_{i,j} \right| \leqslant 10^{-5} \tag{14}$$

The developed code is essentially a modified version of a code built and validated in previous work [14,27]. To check the accuracy of the code for the present problem and the results reported hereafter, energy balance has been employed since no experimental or numerical results were reported for this problem.

The energy balance requires that the heat lost by the lower hot portion must be equal to the heat transferred to the upper cold portion plus the heat being carried out by the fluid at the downstream end. The heat source and heat sink can be written in the present formulation as:

$$\dot{Q}_{\text{source}} = \int_{-1}^{1} \left(-\frac{\partial \theta_{\text{f}}}{\partial Y} \right)_{Y=0} \mathrm{d}X + \frac{1}{K_{\text{r}}} \int_{-1}^{1} \left(-\frac{\partial \theta_{\text{s}}}{\partial Y} \right)_{Y=0} \mathrm{d}X \tag{15a}$$

The heat sink depends upon if there is a cross flow or not. In the case when there is no cross flow ($M = 0$) the heat and flow is symmetrical around y-axis. In this case the heat sink is the upper boundary and the two exits of the fluid and defined as:

$$\dot{Q}_{\text{sink}} = \int_{-(1+S)}^{1+S} \left(-\frac{\partial \theta_{\text{f}}}{\partial Y} \right)_{Y=1} \mathrm{d}X + \frac{1}{K_{\text{r}}} \int_{-(1+S)}^{1+S} \left(-\frac{\partial \theta_{\text{s}}}{\partial Y} \right)_{Y=1} \mathrm{d}X + 2Pe \int_{0}^{1} \left(\frac{\partial \Psi}{\partial Y} \theta \right)_{1+S} \mathrm{d}Y \quad \text{when } M = 0 \tag{15b}$$

While in the case when $M \neq 0$ the heat sink is the upper boundary and the one exits of the fluid and defined as:

$$\dot{Q}_{\text{sink}} = \int_{-(1+S)}^{1+S} \left(-\frac{\partial \theta_{\text{f}}}{\partial Y} \right)_{Y=1} \mathrm{d}X + \frac{1}{K_{\text{r}}} \int_{-(1+S)}^{1+S} \left(-\frac{\partial \theta_{\text{s}}}{\partial Y} \right)_{Y=1} \mathrm{d}X + Pe \int_{0}^{1} \left(\frac{\partial \Psi}{\partial Y} \theta \right)_{1+S} \mathrm{d}Y \quad \text{when } M > 0 \tag{15c}$$

The energy balance has been checked for different flow conditions and $S = 9$ is selected to ensure correct exit boundary conditions (9a) and (9b). Fig. 2 shows the calculated heat source and heat sink during the iteration. At the beginning of the iteration solution, $\dot{Q}_{\text{source}}$ is very large and $\dot{Q}_{\text{sink}}$ is very small because zero initial guess values are used for θ_{f}, θ_{s} and Ψ. An oscillation in the values of $\dot{Q}_{\text{source}}$ and $\dot{Q}_{\text{sink}}$ is found during the iteration and finally the two values converge as the iteration increases, as shown in Fig. 2. The maximum error in the energy balance (the percentage difference between $\dot{Q}_{\text{source}}$ and $\dot{Q}_{\text{sink}}$) is found to be around 2% for different values of the governing parameters.

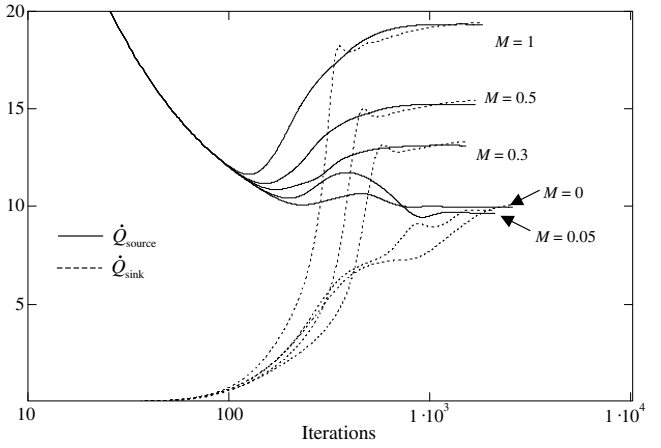

Fig. 2. Variation of the calculated heat source and heat sink during iteration ($H = K_{\text{r}} = 1$ and $Ra = Pe = 100$).

Table 1 shows a comparison of the calculated values of average Nusselt number for both fluid and solid phases at different mesh sizes with $M = 1$ and $Ra = Pe = 100$. It is evident that the (300×40) mesh gives grid independent results, where the differences in the values of the average Nusselt number using (300×40) and (600×80) mesh are less than 2%.

Moreover, to check if S is large enough to ensure correct exit boundary conditions (9a) and (9b), the computational domain is doubled in X-direction, (i.e. $1 + S = 20$) with mesh size doubled also in the horizontal direction, i.e. (600×40). The results show differences less than 0.5% in the values of average Nusselt numbers due to duplication of the computational domain and fixed other parameters.

Table 1
Comparison of the results at different mesh sizes with $M = 1$ and $Ra = Pe = 100$

H	K_{r}	Results with (300×40) mesh		Results with (600×80) mesh	
		$\overline{Nu}_{\text{f}}$	$\overline{Nu}_{\text{s}}$	$\overline{Nu}_{\text{f}}$	$\overline{Nu}_{\text{s}}$
1000	1	6.156	5.282	6.188	5.303
100	1	6.911	4.318	6.929	4.359
10	1	7.700	2.649	7.721	2.685
1	1	8.005	1.638	8.021	1.663
1	10	8.018	2.726	8.046	2.765
1	100	8.037	4.933	8.069	4.991
1	1000	8.048	6.804	8.080	6.841
1000	1000	8.050	8.046	8.082	8.074

Therefore the mesh size (300×40) in the horizontal and vertical directions respectively with $S = 9$ can be considered to give satisfactory good results and adopted for results generation in the next section.

4. Results and discussion

A parametric study is carried out and the results have been obtained to show the effect of the governing parameters on the heat and fluid flow characteristics. The governing parameters and their ranges considered in the present study are: cross flow to jet flow velocity ratio parameter ($0 \leqslant M \leqslant 1$); porosity scaled thermal conductivity ratio parameter ($0.1 \leqslant K_r \leqslant 1000$); heat transfer coefficient parameter ($0.1 \leqslant H \leqslant 1000$); Péclet number ($1 \leqslant Pe \leqslant 1000$) and Rayleigh number with the Darcy model limitations ($10 \leqslant Ra \leqslant 100$). The reader may expect some more parameters, like the jet width and the distance from the jet to the heated surface. The effects of these parameters are studied in details in the recent paper by Saeid and Mohamad [14] and omitted from the present investigation for brevity.

To demonstrate the effect of the cross flow on the heat and fluid flow characteristics, the results are presented in Fig. 3 for local thermal equilibrium conditions with fixed $Ra = Pe = 100$. It is noted from previous studies [19–28] that the local thermal equilibrium condition is satisfied with high values of porosity scaled thermal conductivity ratio parameter and heat transfer coefficient parameter. Fig. 3 shows the effects of imposing different cross flow to jet flow velocity ratio on the streamlines and isotherms for both fluid and solid phases, which are exactly identical, with $H = K_r = 10^3$. Without the presence of the cross flow ($M = 0$), the streamlines and isotherms in Fig. 3a and the local Nusselt number in Fig. 4 show symmetry around the y-axis. A combined effect of jet impingement and cross flow can be observed in Fig. 2b where a counterclockwise rotating cell are formed near the jet due to the presence of the cross flow with $M = 0.05$. For this case ($M = 0.05$), Fig. 4 shows that the local Nusselt number is substantially degraded near $X = 0$ region, where the jet flow and the parallel flow are approximately of same strength. On the other hand, for high values of the cross flow to jet flow velocity ratio (M), Figs. 2d and e show the domination of the parallel flow and vanishing the effect of the jet flow. The variation of the local Nusselt number along the heated portion, shows the usual variation of the parallel flow for the cases with $M = 0.5$ and $M = 1$ as

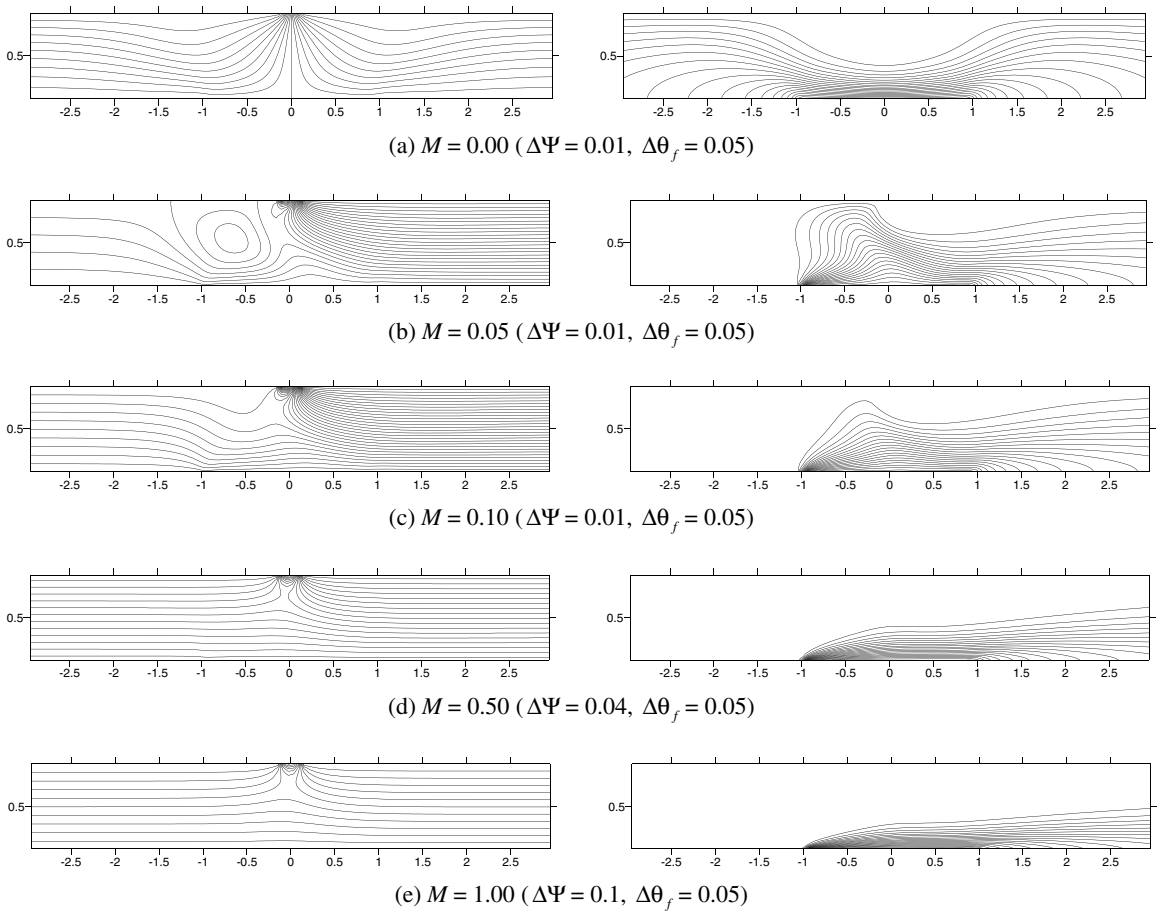

Fig. 3. Streamlines (left) and isotherms (right) for local thermal equilibrium condition with $Ra = Pe = 100$ and $H = K_r = 10^3$ (only important region is shown).

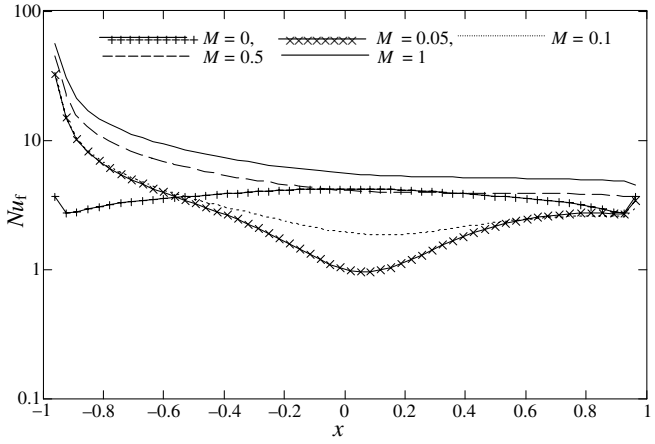

Fig. 4. Variation of local Nusselt number along the heated portion under local thermal equilibrium condition with $Ra = Pe = 100$ and $H = K_r = 10^3$.

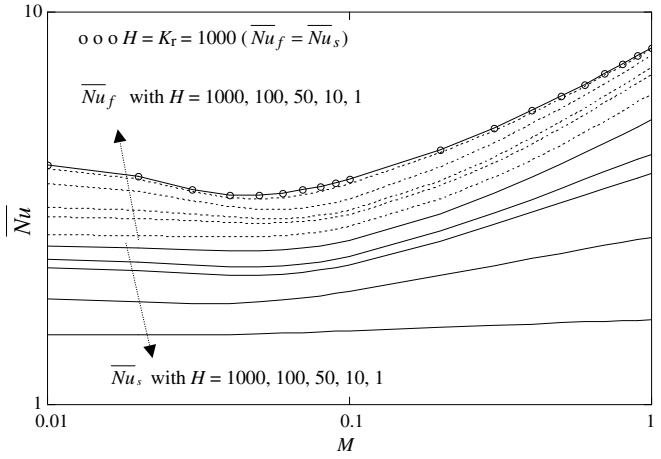

Fig. 6. Variation of average Nusselt numbers with cross flow to jet flow velocity ratio, $K_r = 1$ and $Ra = Pe = 100$.

shown in Fig. 4. The results presented in Figs. 3 and 4 clearly show the lost of the symmetry with the presence of the cross flow.

It is interesting to examine the effect of different values of M on the average Nusselt number under the local thermal non-equilibrium conditions. Figs. 5 and 6 show the effects of local thermal non-equilibrium parameters H and K_r on the variation of average Nusselt number with M for fixed $Ra = Pe = 100$. The results for the local thermal equilibrium conditions ($H = K_r = 10^3$) are presented in Figs. 5 and 6 for comparison. It is interesting to point out that for different local thermal non-equilibrium conditions, the average Nusselt number of the fluid phase shows a minimum values at around $M = 0.05$. The details of the thermal fields of both fluid and solid phases are shown in Fig. 7 for $M = 0.05$ with different local thermal non-equilibrium conditions. It is worth mentioning that the streamlines for these cases are almost same as that presented in Fig. 3b for local thermal equilibrium conditions.

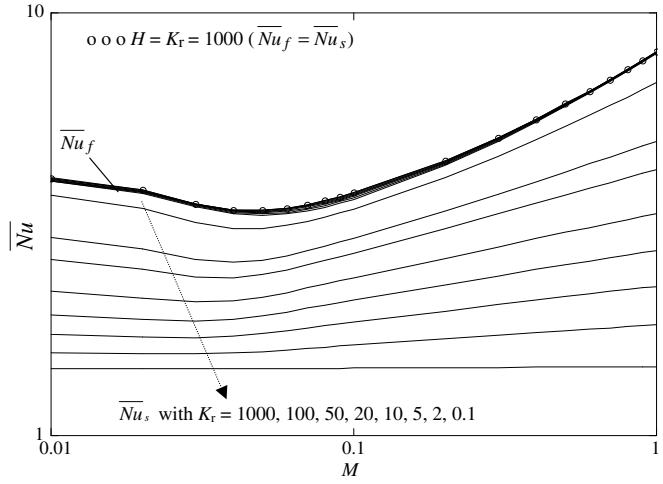

Fig. 5. Variation of average Nusselt numbers with cross flow to jet flow velocity ratio, $H = 1$ and $Ra = Pe = 100$.

The porous medium, with low porosity φ and/or low thermal conductivity of the fluid compared to that of solid, has low thermal conductivity ratio parameter K_r for example the metal foams. In this case the thermal resistance of the solid phase is the minimum and most of the heat will be carried out by conduction through the solid phase and partly by the fluid phase. In this case also, the average Nusselt number of the solid phase is almost constant and not dependent on how much the jet or the cross flow velocity are as shown in Figs. 5 and 6. Increasing the values of K_r leads to the increase in the average Nusselt number of the solid phase and for very high values of K_r the variation of $\overline{Nu}_s$ will approach that of $\overline{Nu}_f$ as shown in Fig. 5. The results presented in Fig. 5 and Table 1 indicate also a slight effect of the porosity scaled thermal conductivity ratio parameter on the variation of $\overline{Nu}_f$ and it is almost same as that for the local thermal equilibrium conditions. This is because the fluid phase temperature field is approximately not affected by the solid phase temperature field with $H = 1$ and different values of K_r as shown in Figs. 7a–c for $M = 0.05$.

Similar variations of $\overline{Nu}_s$ and $\overline{Nu}_f$ with M are shown in Fig. 6 with different values of H and fixed $K_r = 1$ and $Ra = Pe = 100$. At small values of H ($H = 1$), the thermal field in the fluid phase shown in Fig. 7c is approximately same as that under the local thermal equilibrium condition shown in Fig. 3b for $M = 0.05$. Therefore, the values of $\overline{Nu}_f$ is approaching that for the thermally equilibrium model as shown in Fig. 6. Mathematically, as $H \to 0$, Eq. (7) will reduce to the energy equation for fluid phase at the thermally equilibrium model and Eq. (8) will represent the pure conduction equation through the solid phase. Due to this reason, the variation of $\overline{Nu}_s$ with M is approximately constant for $H = 1$ and $K_r = 1$ as shown in Fig. 6. The results show that increasing the heat transfer coefficient parameter leads to reduce $\overline{Nu}_f$ and increase $\overline{Nu}_s$ with fixed other parameters as can be seen from Fig. 6 and Table 1. This is because increasing the heat transfer coefficient between

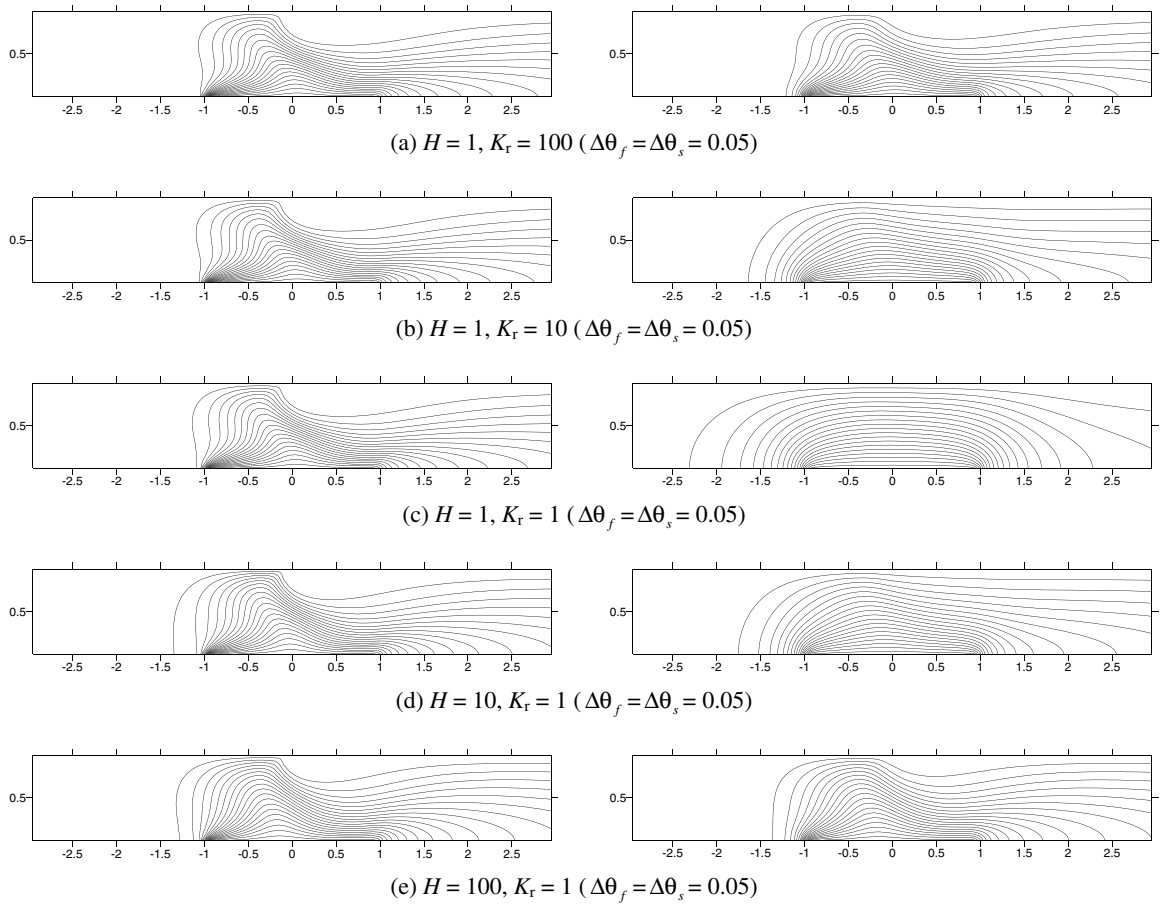

Fig. 7. Isotherms for fluid (left) and soild (right) for local thermal non-equilibrium condition with $M = 0.05$, and $Ra = Pe = 100$.

the solid and the fluid leads to transfer part of the heat from the fluid to the solid matrix in its way from hot region to cold region. This is also obvious by comparing the isotherms of both the solid and the fluid presented in Figs. 7c–e.

It is of practical importance to determine the average total heat transfer (by fluid and solid) per unit area from the heated segment, which can be calculated, by assuming that the surface porosity is equal to the porosity, as:

$$\overline{q''_t} = \frac{1}{2L}\int_{-L}^{L} q''_t(x)\mathrm{d}x = \frac{-1}{2L}\int_{-L}^{L}\left\{\varphi k_f\left(\frac{\partial T_f}{\partial y}\right)_{y=0} + (1-\varphi)k_s\left(\frac{\partial T_s}{\partial y}\right)_{y=0}\right\}\mathrm{d}x \tag{16}$$

The total (effective) average Nusselt number can be defined based on the average total heat transfer, defined in Eq. (16) and overall (effective) thermal conductivity of the porous medium. Kaviany [3] incorporated in his book 13 different definitions for the effective thermal conductivity of the porous medium. In general the weighted arithmetic, harmonic and geometric means of k_f and k_s with weighting factors φ and $(1-\varphi)$ are used, see Nield [31]. The arithmetic mean $k_{eff} = \varphi k_f + (1-\varphi)k_s$ gives the appropriate overall conductivity if the heat conduction in the fluid and solid phases is entirely in parallel. In this case, the total average Nusselt number can be defined as:

$$\overline{Nu_t} = \frac{\overline{q''_t}L}{\Delta T\{\varphi k_f + (1-\varphi)k_s\}} = \frac{-1}{2(K_r+1)}\int_{-1}^{1}\left\{K_r\left(\frac{\partial\theta_f}{\partial Y}\right)_{Y=0} + \left(\frac{\partial\theta_s}{\partial Y}\right)_{Y=0}\right\}\mathrm{d}X \tag{17}$$

The total average Nusselt number is calculated for fixed cross flow ($M = 1$) and different local thermal non-equilibrium conditions to show the effects of Péclet number and Rayleigh number and the results are depicted in Figs. 8 and 9. Fig. 8 shows the variation of $\overline{Nu_t}$ with Pe for both $Ra = 10$ and $Ra = 100$ with different values of H and constant $K_r = M = 1$. In this case, Fig. 8 shows that, for fixed values of H and K_r the difference in the total average Nusselt number (for $Ra = 100$ and $Ra = 10$) is largest for small values of Péclet number (free convection), and this difference diminishes with an increase in Péclet number (forced convection). It is interesting to observe that there is an inflection point (at around $Pe = 10$) in the variation of $\overline{Nu_t}$ with Pe with different values of the heat transfer coefficient parameter shown in Fig. 8. For small values of Péclet number (free convection), the increase of H leads to reduce the variation of $\overline{Nu_t}$ with Pe. In contrast, when the

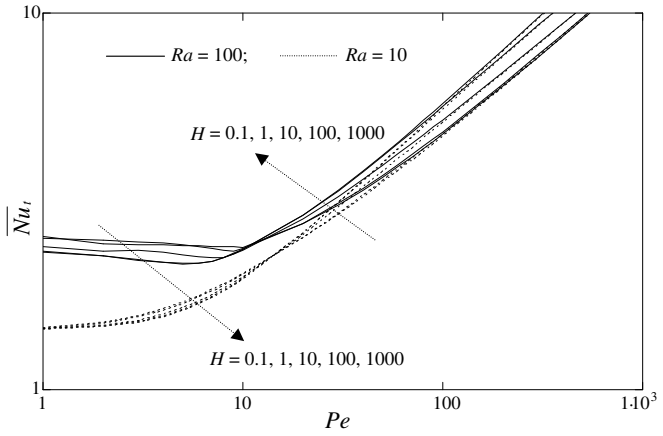

Fig. 8. Variation of total average Nusselt number with Peclet number with $M = 1$ and $K_r = 1$.

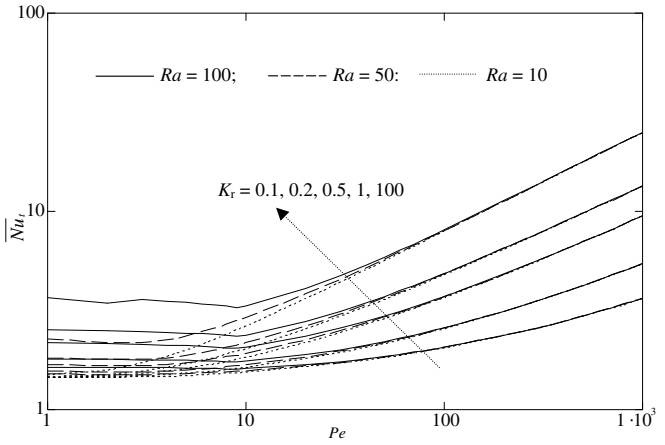

Fig. 9. Variation of total average Nusselt number with Peclet number with $M = 1$ and $H = 1$.

values of Péclet number are high (forced convection), the increase of H leads to increase the values of $\overline{Nu_t}$ as shown in Fig. 8.

The effect of the thermal conductivity ratio parameter on the variation of $\overline{Nu_t}$ with Pe is studied for $Ra = 10$, 50 and 100 and constant $H = M = 1$. As mentioned earlier, the effect of the Rayleigh number is clear only for flows with low values of Péclet number. Fig. 9 shows that the increase of the thermal conductivity ratio parameter leads to a substantial increase in the variation of $\overline{Nu_t}$ in both the free convection and forced convection modes. To have better insight of the effect of Péclet number, the streamlines and isotherms for both fluid and solid phases are presented in Fig. 10 for $Ra = 50$ and $M = H = K_r = 1$. At low values of Péclet number, the free convection heat transfer is dominated, where two opposite rotating cells of the fluid are formed above the heated surface as shown in Fig. 10a. Increasing the Péclet number, the two rotating cells of the fluid become weaker and the external flow from both the jet and the cross flow start to play a role in the heat transfer as shown in Figs. 10b and c. Increasing further the Péclet number leads to the domination of the external flow and diminish the effect of the buoyancy driven flow as shown in Fig. 10d. It is interesting to observe that the

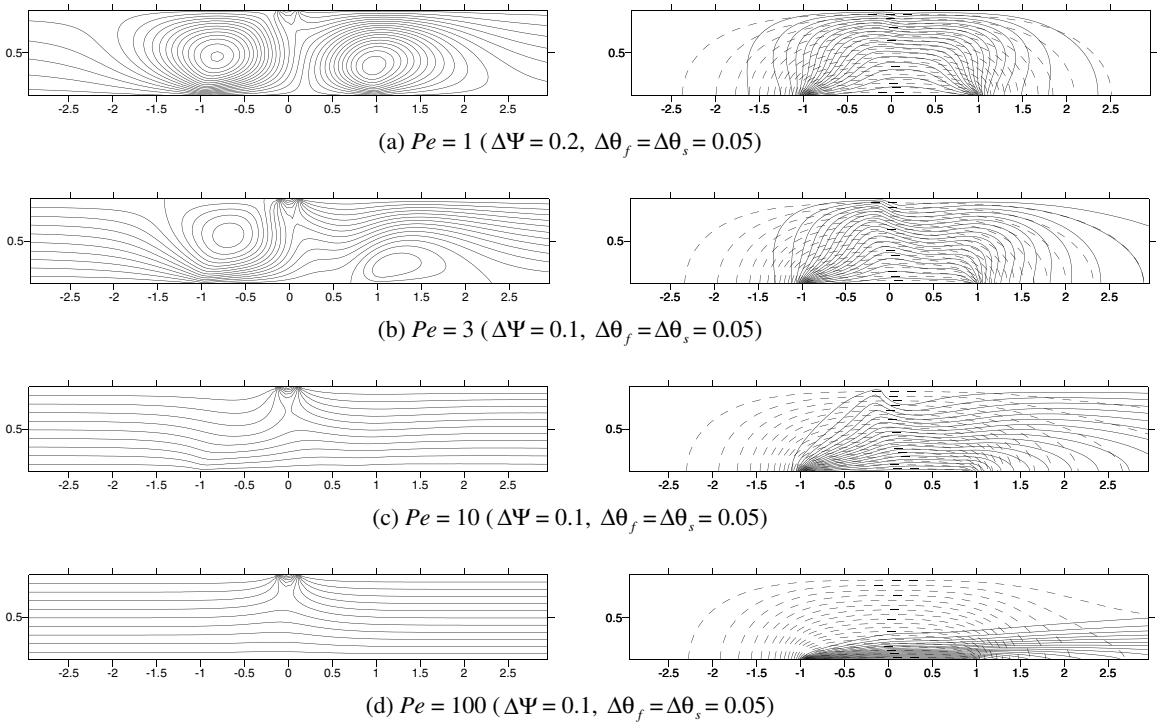

Fig. 10. Streamlines (left) Isotherms (right, solid lines for θ_f and dash lines for θ_s) for local thermal non-equilibrium condition with $M = H = K_r = 1$ and $Ra = 50$.

thermal field of the solid phase is affected with the change in the strength of the external flow.

Finally, it should be mention that oscillatory convection is expected for small values of cross flow ($M < 0.1$) and Péclet number ($Pe < 10$) especially for high values of Rayleigh number ($Ra = 100$) and any value of the local thermal non-equilibrium parameters (H and K_r). The oscillatory convection in porous layer is studied in details for similar problem; see for example, Lai and Kulacki [32] and Saeid and Mohamad [14].

5. Conclusions

The interaction of a vertical jet and a horizontal cross flow cooling of a horizontal surface immersed in a fluid saturated porous media is investigated numerically under local thermal non-equilibrium conditions. The mathematical model is derived for steady, two-dimensional laminar flow based on Darcy model and two-energy equation for fluid and solid phases. The governing parameters and their ranges considered in the present parametric study are: cross flow to jet flow velocity ratio parameter ($0 \leqslant M \leqslant 1$); porosity scaled thermal conductivity ratio parameter ($0.1 \leqslant K_r \leqslant 1000$); heat transfer coefficient parameter ($0.1 \leqslant H \leqslant 1000$); Péclet number ($1 \leqslant Pe \leqslant 1000$) and Rayleigh number with the Darcy model limitations ($10 \leqslant Ra \leqslant 100$). The total average Nusselt number is defined based on the overall thermal conductivity, which is assumed to be the arithmetic mean of the porosity scaled thermal conductivity of the fluid and solid phases. The total average Nusselt number as well as the average Nusselt number for both fluid and solid phases is presented for different governing parameters. Without the presence of the cross flow ($M = 0$), the local Nusselt number and the fluid and heat flow show symmetry around the centerline of the jet. Imposing cross flow with small velocity ratio ($M = 0.05$), the local Nusselt number is substantially degraded near $X = 0$ region, where the jet flow and the parallel flow are approximately of same strength. On the other hand, for high values of the cross flow to jet flow velocity ratio (M); the results show the domination of the parallel flow and vanishing the effect of the jet flow. The results show that, the average Nusselt number calculated from the thermal equilibrium model are the maximum possible values and these values can be reproduced by large values of $H \times K_r$.

References

[1] D.A. Nield, A. Bejan, Convection in Porous Media, third ed., Springer, New York, 2006.

[2] K. Vafai (Ed.), Handbook of Porous Media, second ed., Taylor & Francis, New York, 2005.

[3] M. Kaviany, Principles of Heat Transfer in Porous Media, second ed., Springer, New York, 1995.

[4] I. Pop, D.B. Ingham, Convective Heat Transfer: Mathematical and Computational Modelling of Viscous Fluids and Porous Media, Pergamon, Oxford, 2001.

[5] S. Al-Sanea, A numerical study of the flow and heat transfer characteristics of an impinging laminar slot-jet including crossflow effects, Int. J. Heat Mass Transfer 35 (1992) 2501–2513.

[6] F.J. Higuera, M. Martinez, An incompressible jet in a weak crossflow, J. Fluid Mech. 249 (1993) 73–97.

[7] A.J. Humber, E.W. Grandmaison, A. Pollard, Mixing between a sharp-edged rectangular jet and a transverse cross flow, Int. J. Heat Mass Transfer 36 (1993) 4307–4316.

[8] L.B.Y. Aldabbagh, I. Sezai, A.A. Mohamad, Three-dimensional investigation of a laminar impinging square jet interaction with crossflow, ASME J. Heat Transfer 125 (2003) 243–249.

[9] D.H. Lee, J. Song, M.C. Jo, The effects of nozzle diameter on impinging jet heat transfer and fluid flow, ASME J. Heat Transfer 126 (2004) 554–557.

[10] X. Li, J.L. Gaddis, T. Wang, Multiple flow patterns and heat transfer in confined jet impingement, Int. J. Heat Fluid Flow 26 (2005) 746–754.

[11] W.S. Fu, H.C. Huang, Thermal performance of different shape porous blocks under an impinging jet, Int. J. Heat Mass Transfer 40 (1997) 2261–2272.

[12] M. Prakash, O.F. Turan, Y. Li, J. Mahoney, G.R. Thorpe, Impinging round jet studies in a cylindrical enclosure with and without a porous layer: Part I – Flow visualizations and simulations, Chem. Eng. Sci. 56 (2001) 3855–3878.

[13] T.M. Jeng, S.C. Tzeng, Numerical study of confined slot jet impinging on porous metallic foam heat sink, Int. J. Heat Mass Transfer 48 (2005) 4685–4694.

[14] N.H. Saeid, A.A. Mohamad, Jet impingement cooling of a horizontal surface in a confined porous medium: mixed convection regime, Int. J. Heat Mass Transfer 49 (2006) 3906–3913.

[15] N.H. Saeid, A.A. Mohamad, Jet impingement on a discrete heater in a thermally non-equilibrium porous layer, Paper Number 1, in: 3rd International Conference Applications of Porous Media, May 29–June 3rd, 2006, Marakish, Morocco, pp. 1–7.

[16] A.A. Mohamad, S. Ramadhyani, R. Viskanta, Modelling of combustion and heat transfer in a packed bed with embedded coolant tubes, Int. J. Heat Mass Transfer 37 (1994) 1181–1197.

[17] K. Vafai, M. Sozen, Analysis of energy and momentum transport for fluid flow through a porous bed, ASME J. Heat Transfer 112 (1990) 690–699.

[18] T.E.W. Schumann, Heat transfer: a liquid flowing through a porous prism, J. Franklin Instit. 208 (1929) 405–416.

[19] A. Amiri, K. Vafai, Analysis of dispersion effects and non-thermal equilibrium, non-Darcian, variable porosity incompressible flow through porous media, Int. J. Heat Mass Transfer 37 (1994) 939–954.

[20] A. Amiri, K. Vafai, Transient analysis of incompressible flow through a packed bed, Int. J. Heat Mass Transfer 41 (1998) 4259–4279.

[21] W.J. Minkowycz, A. Haji-Sheikh, K. Vafai, On departure from local thermal equilibrium in porous media due to a rapidly changing heat source: the Sparrow number, Int. J. Heat Mass Transfer 42 (1999) 3373–3385.

[22] P.X. Jiang, Z.P. Ren, Numerical investigation of forced convection heat transfer in porous media using a thermal non-equilibrium model, Int. J. Heat Fluid Flow 22 (2001) 102–110.

[23] S.J. Kim, S.P. Jang, Effect of the Darcy number, the Prandtl number, and the Reynolds number on local thermal non-equilibrium, Int. J. Heat Mass Transfer 45 (2002) 3885–3896.

[24] N. Banu, D.A.S. Rees, Onset of Darcy–Benard convection using a thermal non-equilibrium model, Int. J. Heat Mass Transfer 45 (2002) 2221–2228.

[25] A.C. Baytas, I. Pop, Free convection in a square porous cavity using a thermal nonequilibrium model, Int. J. Therm. Sci. 41 (2002) 861–870.

[26] A.A. Mohamad, Natural convection from a vertical plate in a saturated porous medium, non-equilibrium theory, J. Porous Media 4 (2001) 181–186.

[27] N.H. Saeid, Analysis of mixed convection in a vertical porous layer using non equilibrium model, Int. J. Heat Mass Transfer 47 (2004) 5619–5627.

[28] N.H. Saeid, A.A. Mohamad, Periodic free convection from a vertical plate in a saturated porous medium, non-equilibrium model, Int. J. Heat Mass Transfer 48 (2005) 3855–3863.
[29] S.V. Patankar, Numerical Heat Transfer and Fluid Flow, McGraw-Hill, New York, 1980.
[30] T. Hayase, J.A.C. Humphrey, R. Greif, A consistently formulated QUICK scheme for fast and stable convergence using finite-volume iterative calculation procedures, J. Comput. Phys. 98 (1992) 108–118.
[31] D.A. Nield, Estimation of the stagnant thermal conductivity of saturated porous media, Int. J. Heat Mass Transfer 34 (1991) 1575–1576.
[32] F.C. Lai, F.A. Kulacki, Oscillatory mixed convection in horizontal porous layers heated from below, Int. J. Heat Mass Transfer 34 (1991) 887–890.